Regular Article

PHYSICAL CHEMISTRY RESEARCH
Published by the
Iranian Chemical Society
www.physchemres.org
info@physchemres.org

Phys. Chem. Res., Vol. 9, No. 3, 385-412, September 2021
DOI: 10.22036/pcr.2021.264541.1869

Pharmacokinetics and Molecular Docking Studies of Uridine Derivatives as SARS-COV-2 M^{pro} Inhibitors

J. Maowa[a], M.A. Hosen[a], A. Alam[a], K.M. Rana[a], Y. Fujii[b], Y. Ozeki[c] and S.M.A. Kawsar[a,*]

[a]*Laboratory of Carbohydrate and Nucleoside Chemistry, Department of Chemistry, Faculty of Science, University of Chittagong, Chittagong-4331, Bangladesh*

[b]*Laboratory of Functional Morphology, Graduate School of Pharmaceutical Sciences, Nagasaki International University, 2825-7 Huis Ten Bosch, Sasebo, Nagasaki 859-3298, Japan*

[c]*Laboratory of Glycobiology and Marine Biochemistry, Department of Life and Environmental System Science, Graduate School of NanoBiosciences, Yokohama City University, 22-2 Seto, Kanazawa-ku, Yokohama 236-0027, Japan*

(Received 27 December 2020, Accepted 7 April 2021)

Various clinical trials are undergoing to identify specific drugs for the treatment of new global threat viruses. The main protease of SARS-CoV-2 is one of the significant targets to design and amplify antiviral drugs. In this investigation, we optimized a nucleoside, uridine, and some of its acylated derivatives (2-14) using density functional theory (DFT) at the B3LYP/3-21G level of theory. Charge distribution, polarizability, and thermodynamic properties such as free energy, heat capacity, entropy, of modified compounds were studied in the subsequent analysis to evaluate how certain groups (aliphatic and aromatic) impact the drug properties. It was observed that all derivatives were thermodynamically more stable than the parent ligand, uridine, and some of them were more chemically reactive than others. Then, molecular docking was performed against SARS-CoV-2 main protease (PDB: 6Y84 and 6LU7) to investigate the binding mode (s) and binding affinities of the selected uridine derivatives. Most of the compounds studied here could bind near the crucial catalytic residues, HIS41 and CYS145 of the main protease and surrounded by other active site residues such as GLY143, MET49, MET165, HIS163, PRO168, GLU166, GLN189 and SER144. Significant binding affinities (-6.0 to -7.8 kcal mol^{-1}) for 6LU7 and (-5.9 to -7.7 kcal mol^{-1}) for 6Y84 were found which revealed the potency of inhibition of uridine derivatives against SARS-CoV-2 M^{pro}. Finally, all the modified uridine derivatives were analyzed *in silico* ADMET and drug-like properties. Overall, the present study could be helpful for the development of uridine-based novel potential inhibitors against the SARS-CoV-2 M^{pro}.

Abbreviations: DFT: Density Functional Theory; ADMET: Absorption, Distribution, Metabolism, Excretion, and Toxicity; QM: Quantum Mechanical; LYP: Lee, Yang and Parr's; NBO: Natural Bond Orbitals; MEP: Molecular electrostatic potential; hERG: Human Ether-A-Go-Go-Related Gene; BBB: Blood Brain Barrier.

Keywords: DFT, Molecular docking, Pharmacokinetic, SARS-COV-2 M^{pro}, Uridine

INTRODUCTION

Uridine (1) derivatives have a potential inhibitory function against 3C-like protease protein [1,2]. Azidothymidine, indinavir and tipranavir are the well-known nucleoside centered antiviral drugs [3]. Uridine, with the molecular formula $C_9H_{12}N_2O_6$, is a pyrimidine nucleoside-analog in which uracil is attached to a ribose ring *via* a β-N_1-glycosidic bond. It is a vital element for the synthesis of RNA and biomembranes and for the regulation of normal physiological processes [4]. It also helps create phospholipids in the brain. Synthesis and degradation of

*Corresponding author. E-mail: akawsarabe@yahoo.com

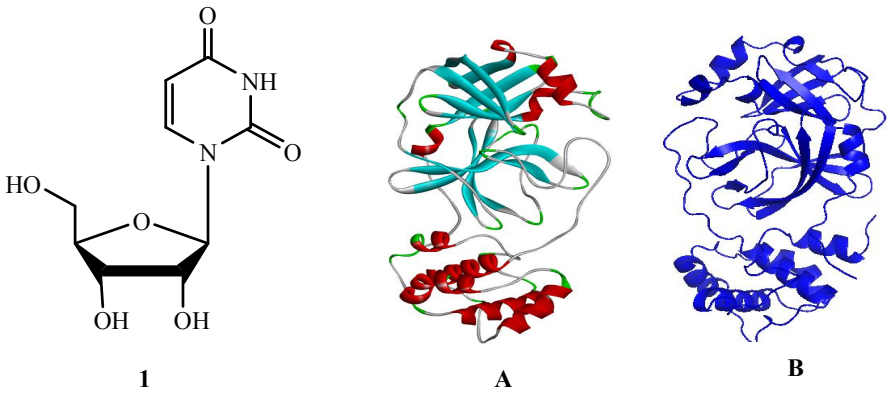

Fig. 1. Structure of uridine (1) and crystal structures of main protease 6LU7 (A) and 6Y84 (B).

uridine in the liver play the main roles in controlling its plasma concentration [5]. Uridine seems to have an important role in the initiation and success of human reproduction. Uridine at a high concentration in seminal plasma was found to have a positive correlation to the ratio of motile spermatozoa in men with normal and abnormal spermiogram findings. This result indicates that the optimal secretory function of uridine may be associated with an increased percentage of spermatozoa with better motility [6]. Recently, it was demonstrated that uridine increased the biosynthesis of hyaluronic acid in cultured corneal epithelial cells and keratinocytes, while it also enhanced corneal wound healing and increased the number of conjunctival goblets cells in rabbits *in vivo* [7].

Computational chemistry is a tool that helps to predict physicochemical, spectral, and biological properties of newly synthesized chemicals [8,9]. In this study, we have replaced the hydroxyl (-OH) group of uridine by different aliphatic and aromatic groups and these designed derivatives are optimized to realize their thermochemical and biochemical behavior based on quantum mechanical methods. The free energy, entropy, heat capacity, polarizability, atomic partial charges have been calculated to compare their thermal and chemical characteristic. It helps to determine if a particular reaction will occur and if it will release or absorb energy as it occurs. The recent outbreak of a novel coronavirus disease (CoViD-19) causes a severe acute respiratory syndrome (SARS). The rapid spread of this kind of virus has raised CoViD-19 to the rank of a global pandemic [10]. Here, molecular docking is performed on a receptor protein of SARS-CoV-2 main protease (PDB: 6Y84 and 6LU7) (Fig. 1) in order to identify the binding mode and affinity and non-binding interaction of designed uridine derivatives (Fig. 2) with the receptor protein. Furthermore, to highlight the drug-like properties, the standard pharmacokinetic parameters (ADMET) have been predicted *in silico*. This study is focused on the identification of uridine derivatives (Fig. 2) with the aim to expedite the identification of specific drugs for the treatment of COVID-19.

EXPERIMENTAL

Materials

To investigate the drug interactions with receptor proteins, molecular docking methods are the best suitable tools. The blind docking method employs a search throughout the whole surface of the protein molecule for binding sites. So, blind molecular docking studies of some bioactive organic compounds; *i.e.*, uridine derivatives (Fig. 2), have been screened with the main protease of COVID-19. The following softwares were used in the present study: i) Gaussian 09, ii) GaussSum 3.0, iii) AutoDock 4.2.6, iv) Swiss-Pdb 4.1.0, v) Python 3.8.2, vi) Discovery Studio 3.5, vii) PyMOL 2.3, viii) ChemDraw Pro 12.0 was used to draw the two-dimensional structure of uridine derivatives ix) pkCSM server (http://biosig.unimelb.edu.au) and SwissADME free web tools (http://www.swissadme.ch) were employed to calculate the pharmacokinetic properties.

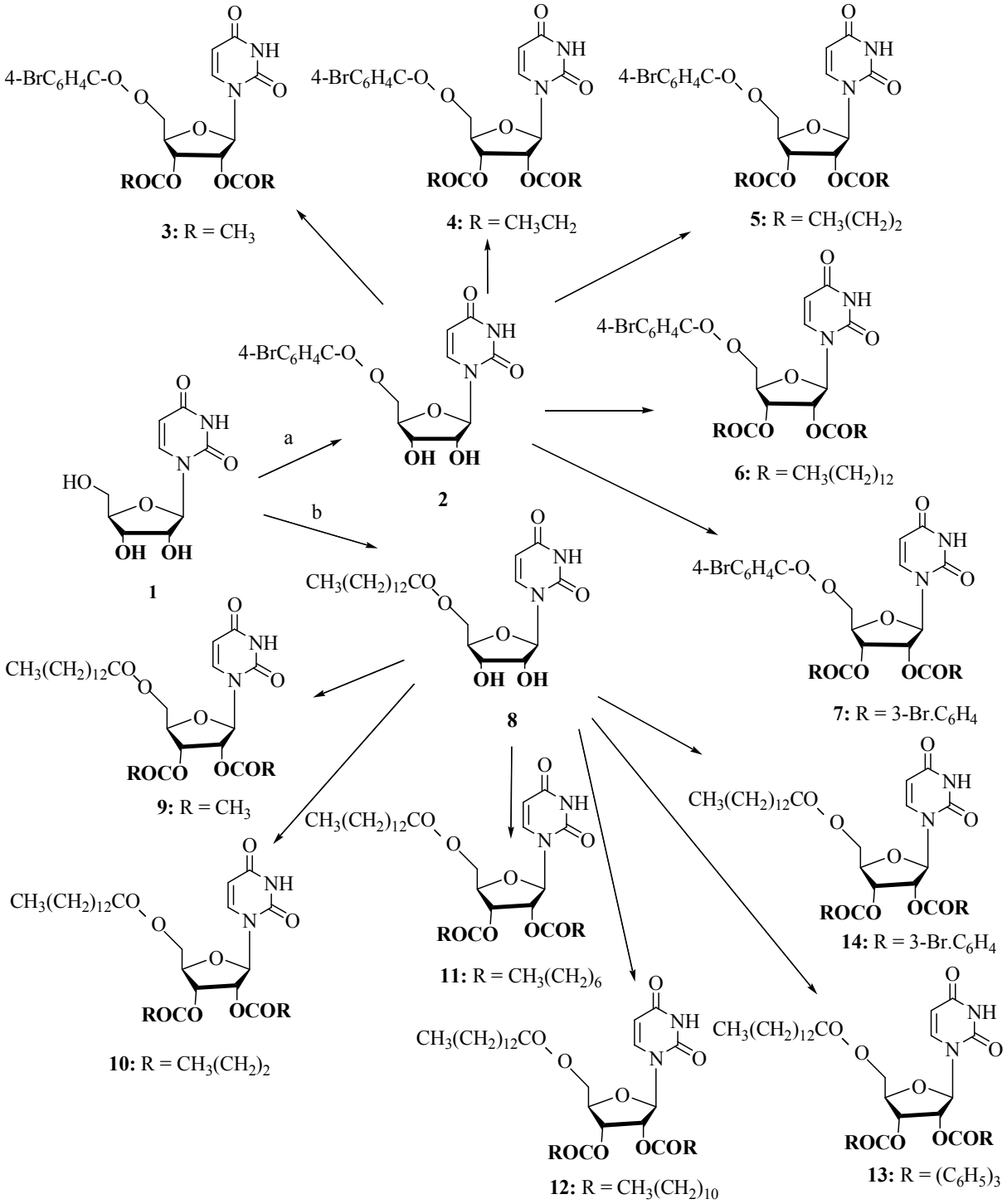

Fig. 2. Chemical structure of uridine (1) and its derivatives (2-14).

Strategies and Visualization of Designed Uridine Derivatives

The newly modified derivatives of uridine (Fig. 2) used in this study were designed according to the reactions scheme.

Computational Details

Optimization of uridine derivatives. In computational chemistry, quantum mechanical methods are widely used to calculate thermal, molecular orbital and molecular electrostatic properties [11]. Geometry optimizations of all designed derivatives are carried out using the Gaussian 09 program [11]. Density functional theory (DFT) with Beck's (B) [12] three-parameter hybrid model, Lee, Yang and Parr's (LYP) [13] correlation functional under 3-21G basis set was used to optimize and predict their thermal and molecular orbital properties. Free energy, entropy, heat capacity, and polarizability were calculated for all the compounds considering the Parr and Pearson's interpretation of DFT and Koopmans theory [14] on the correlation of ionization potential (I) and electron affinities (E) with HOMO and LUMO energy (ε).

Geometry Optimization Plot

In the field of computational chemistry, energy minimization is the process to identify an extended array of atoms in space where the net inter-atomic force on each atom is acceptably close to zero and the position on the potential energy surface (PES) is a stationary point.

Geometry optimization structure can be used for theoretical investigations in the fields of chemical structure, thermodynamics, chemical kinetics, spectroscopy and others. Another important method for exploring these energy surfaces is to find configurations for which the energy is a minimum. This means finding a point in configuration space where all forces on the atoms are balanced. By simply minimizing the energy of a molecule, stable conformations are identified. To determine the optimization plots, all the optimized uridine derivatives (Gaussian output file) were converted into txt files by notepad. Then, the txt files became input for the GaussSum 3.0 software to get desired curves. Finally, minimized energy and the deviation from targets with the optimization steps were calculated from the predicted plots.

In Silico Pharmacokinetics ADMET and Drug-Like Parameters Prediction

To point out potential drug candidates, the ADMET properties were developed for the preliminary prediction of the pharmacokinetic and physicochemical, and drug-like properties in the discovery drug process. *In silico* study gives a way to access the pharmacokinetic parameters (ADMET) [15], its absorption in the human intestine, percolation of the blood-brain barrier and the central nervous system. The metabolism indicates the chemical biotransformation of a drug by body, total clearance of drugs and the toxicity levels of the molecules. The drug likeliness of a molecule is expressed by Lipinski's rule of five parameters (molecular weight < 500 Da, no more than five hydrogen bond donors, number of hydrogen bond acceptors should be less than 10 and logP should not be greater than 5). Lipinski's rule of five properties was obtained from the SwissADME server (www.swissadme.ch/index.php) [16]. The chemical structures, chemical formula, and Lipinski's rule parameters of the ligands are listed in Table 6.

Structure, Preparation of M^{pro} and Molecular Docking

The 3D structure of SARS-CoV-2 M^{pro} (PDB ID. 6Y84 and 6LU7) was collected in pdb format from the protein data bank [17]. All hetero atoms and water molecules were taken away by using PyMol (version 1.3) software packages [18]. Swiss-Pdb viewer software (version 4.1.0) was employed for energy minimization of the protein [19]. Then, the optimized drugs were subjected to molecular docking study against SARS-CoV-2 M^{pro} protein (6Y84 and 6LU7). Molecular docking simulation was rendered by PyRx software (version 0.8) [20] considering the protein as a macromolecule and the drug as a ligand. AutodockVina was employed for docking analysis, and AutoDock Tools (ADT) of the MGL software package was used to convert pdb into a pdbqt format to input protein and ligands. The size of grid box in AutoDockVina in the case of receptor protein 6Y84 was kept at 38.0853, 66.5301 and 63.5733Å for X, Y, Z directions, respectively. Again, it was kept at 51.3565, 66.9335 and 59.6050 Å for 6LU7. After completing docking, both the macromolecule and ligand structures were saved in pdbqt format needed by Accelrys

Table 1. List of the Uridine Derivatives (2-14)

Entry	Name of the compounds	Acyl groups (5′-*O*-)	Acyl groups (2′,3′-Di-*O*-)
1	Uridine	–	–
2	5′-*O*-(4-Bromobenzoyl)uridine	4-BrC_6H_4CO-	–
3	2′,3′-Di-*O*-acetyl-5′-*O*-(4-bromobenzoyl)uridine	4-BrC_6H_4CO-	CH_3CO-
4	5′-*O*-(4-Bromobenzoyl)-2′,3′-di-*O*-propionyluridine	4-BrC_6H_4CO-	CH_3CH_2CO-
5	5′-*O*-(4-Bromobenzoyl)-2′,3′-di-*O*-butyryluridine	4-BrC_6H_4CO-	$CH_3(CH_2)_2$CO-
6	5′-*O*-(4-Bromobenzoyl)-2′,3′-di-*O*-myristoyluridine	4-Br.C_6H_4CO-	$CH_3(CH_2)_{12}$CO-
7	2′,3′-Di-*O*-(3-bromobenzoyl)-5′-*O*-(4-bromobenzoyl)uridine	4-Br.C_6H_4CO-	3-Br.C_6H_4CO-
8	5′-*O*-Myristoyluridine	$CH_3(CH_2)_{12}$CO-	–
9	2′,3′-Di-*O*-acetyl-5′-*O*-myristoyluridine	$CH_3(CH_2)_{12}$CO-	CH_3CO-
10	2′,3′-Di-*O*-butyryl-5′-*O*-myristoyluridine	$CH_3(CH_2)_{12}$CO-	$CH_3(CH_2)_2$CO-
11	5′-*O*-Myristoyl-2′,3′-di-*O*-octanoyluridine	$CH_3(CH_2)_{12}$CO-	$CH_3(CH_2)_6$CO-
12	2′,3′-Di-*O*-lauroyl-5′-*O*-myristoyluridine	$CH_3(CH_2)_{12}$CO-	$CH_3(CH_2)_{10}$CO-
13	5′-*O*-Myristoyl-2′,3′-di-*O*-trityluridine	$CH_3(CH_2)_{12}$CO-	$(C_6H_5)_3$C-
14	2′,3′-Di-*O*-(3-bromobenzoyl)-5′-*O*-myristoyluridine	$CH_3(CH_2)_{12}$CO-	3-Br.C_6H_4CO-

Discovery Studio (version 4.1) to explore and visualize the docking result and search the non-bonding interactions between ligands and amino acid residues of receptor protein [21].

RESULTS AND DISCUSSION

In the present study, thirteen uridine derivatives with different aliphatic and aromatic chains (2-14) (Table 1) were designed, and a quantum chemical study was performed to realize the mode of their thermochemical properties. According to the nature of the substituents, designed uridine esters were distinguished as aliphatic chains (2-6, 8-12), and aromatic rings (7, 13 and 14) to clarify the variation of properties. The observed activities were then rationalized by molecular docking, and with the combination ADMET and drug-likeness properties.

Optimization Plot Analysis

Optimization of energy systems comprehensively describes the thermodynamic modeling, analysis and optimization of numerous types of energy systems in various applications. It provides a new understanding of the system and the process of defining proper objective functions for determination of the most suitable design parameters for achieving enhanced efficiency. The energy minimization plots (Fig. 3) of the designed uridine derivatives indicated that energy minimization occurred more smoothly in case of modified derivatives than the parent ligand (1). Uridine esters (2-6) substituted by 4-bromobenzoyl and different aliphatic groups (C2-C16) showed a smooth increase of minimized energy as the

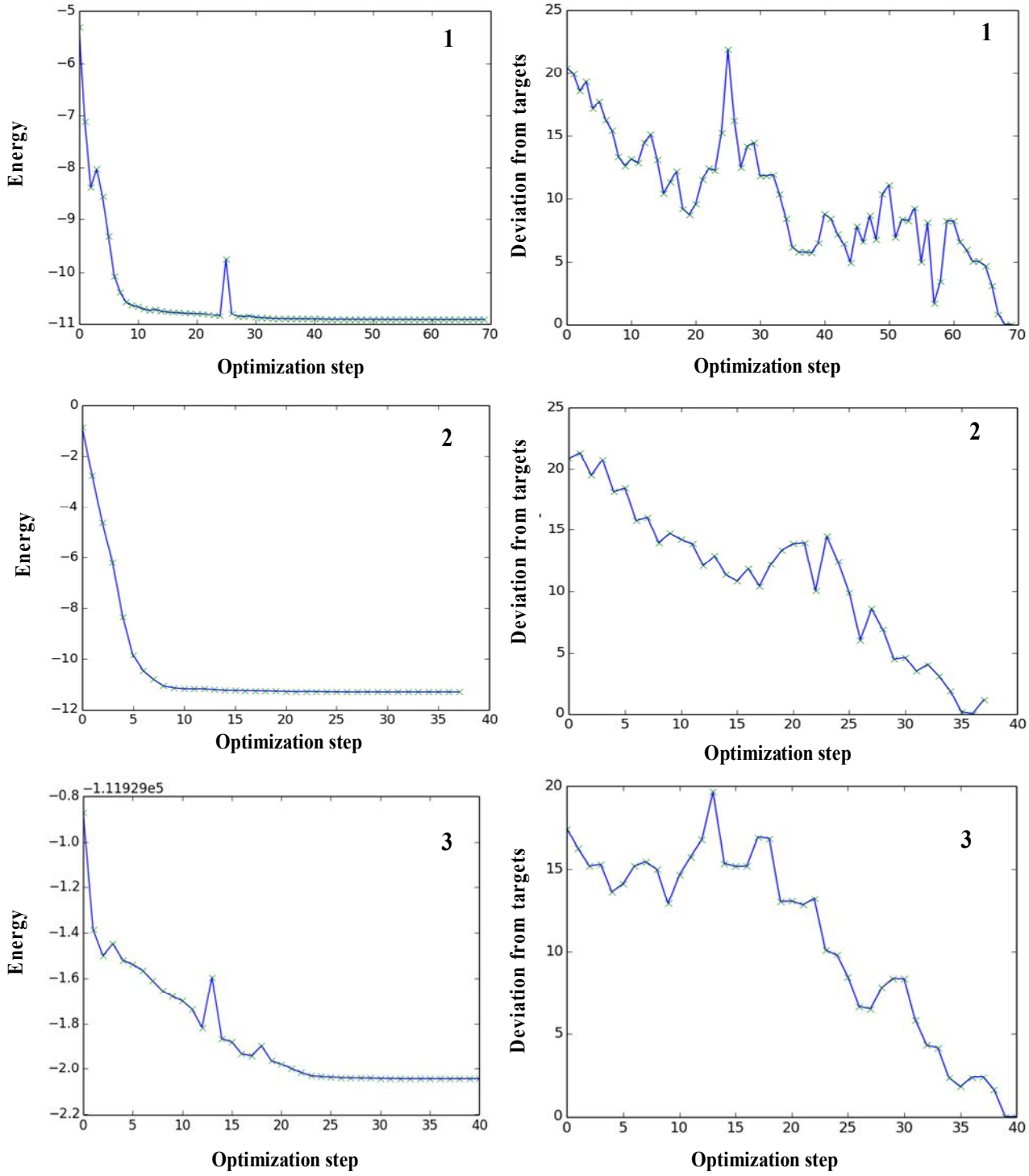

Fig. 3. Geometrical optimization curve of uridine (1) and its derivatives (2-14).

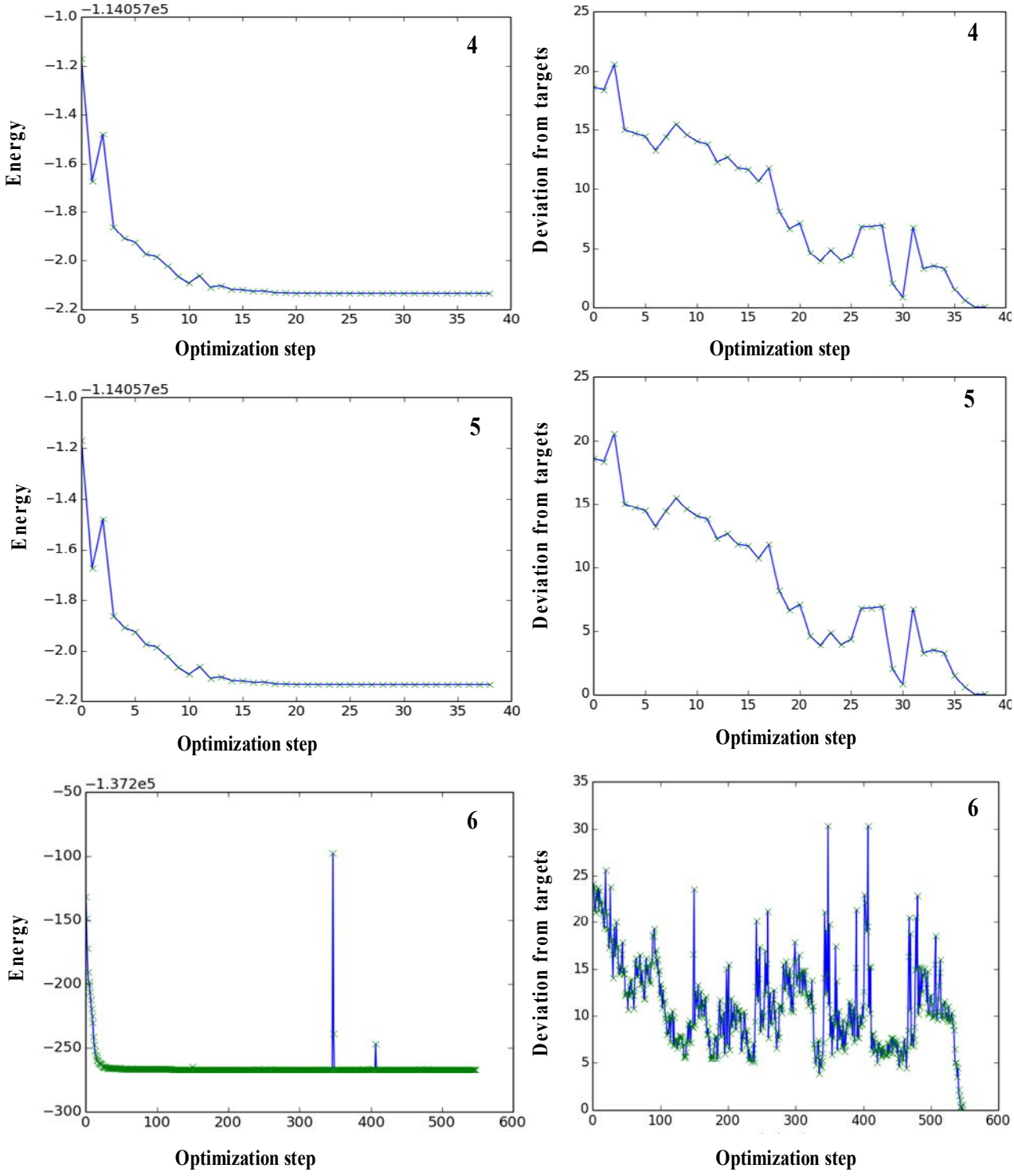

Fig. 3. Continued.

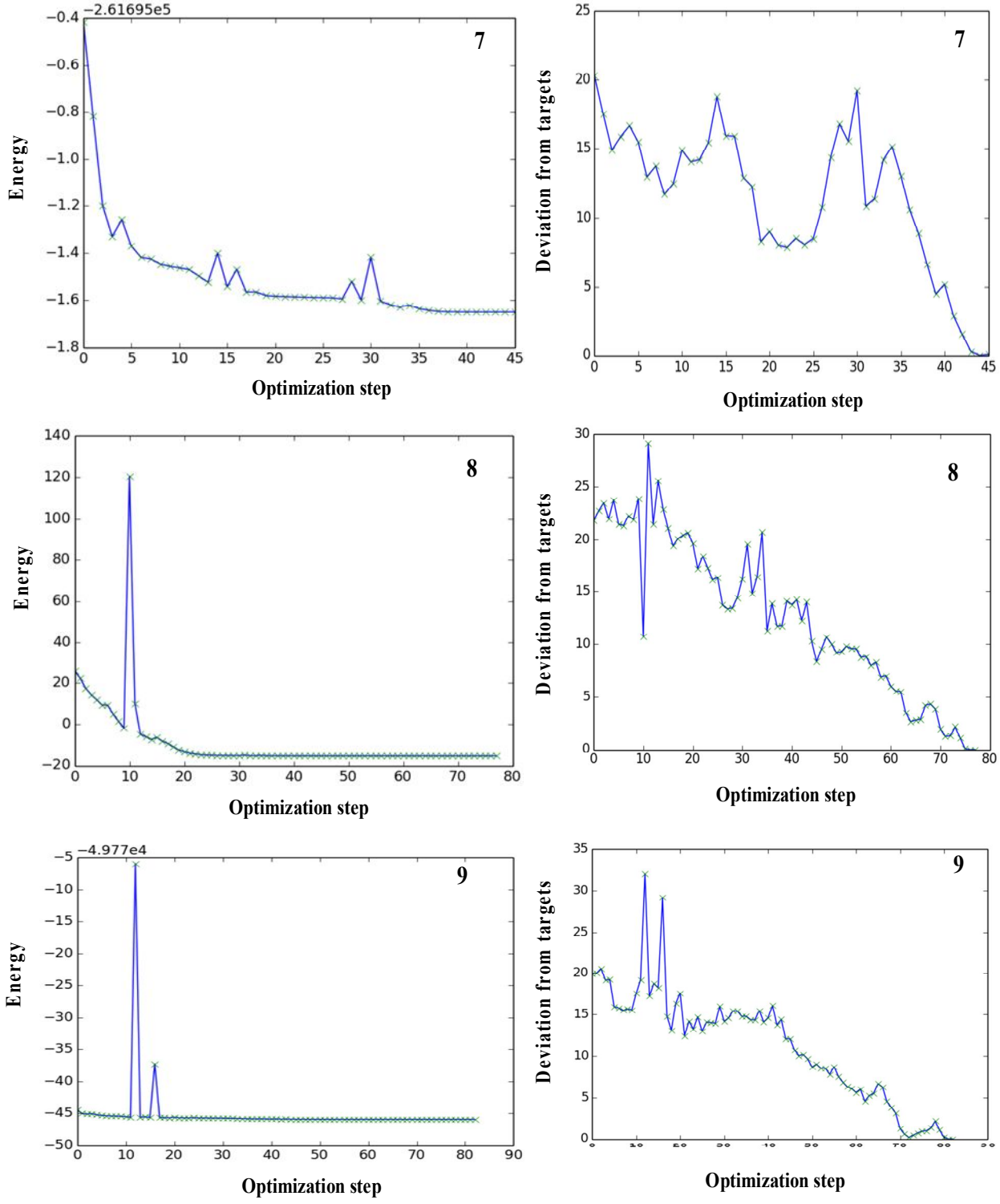

Fig. 3. Continued.

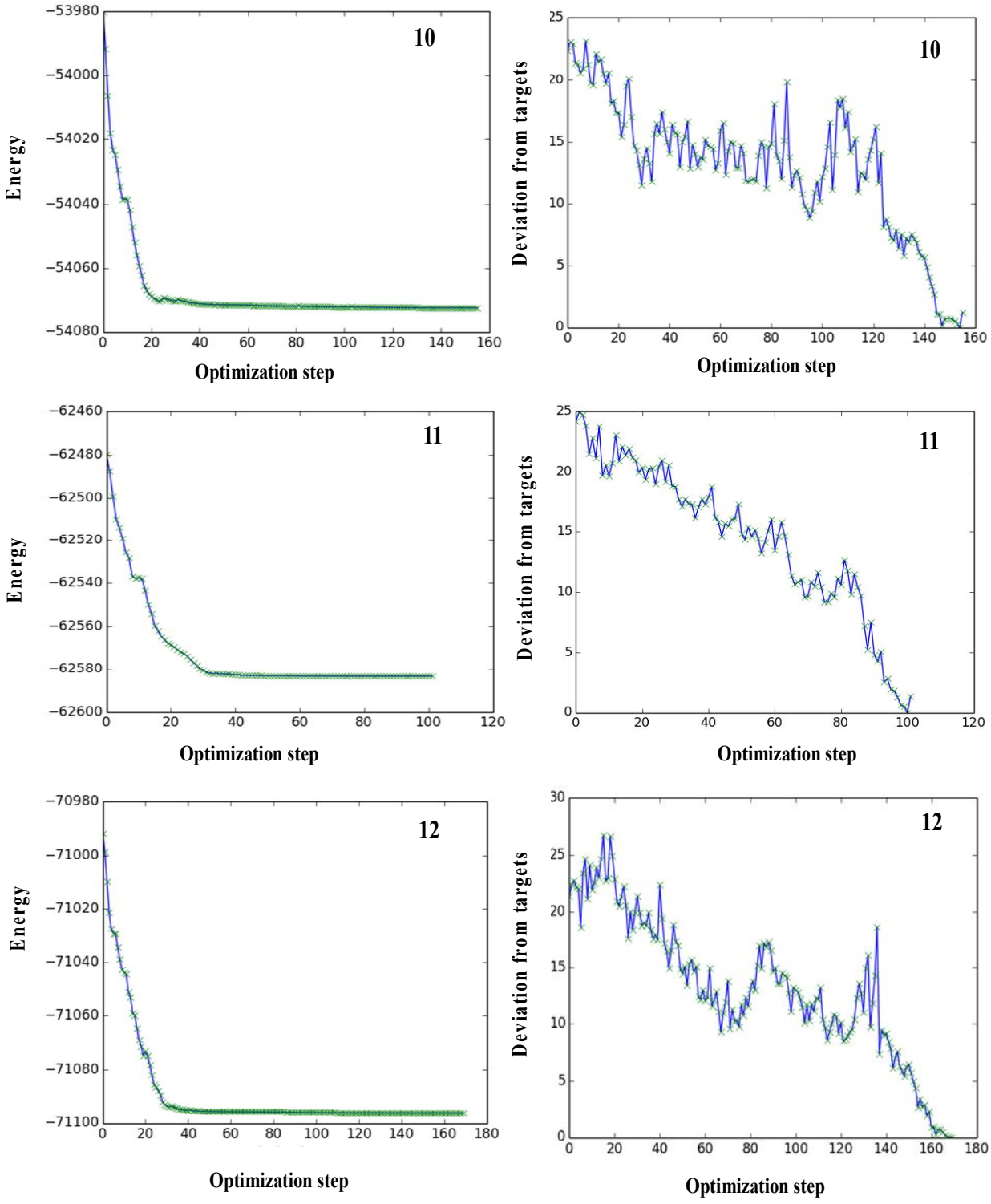

Fig. 3. Continued.

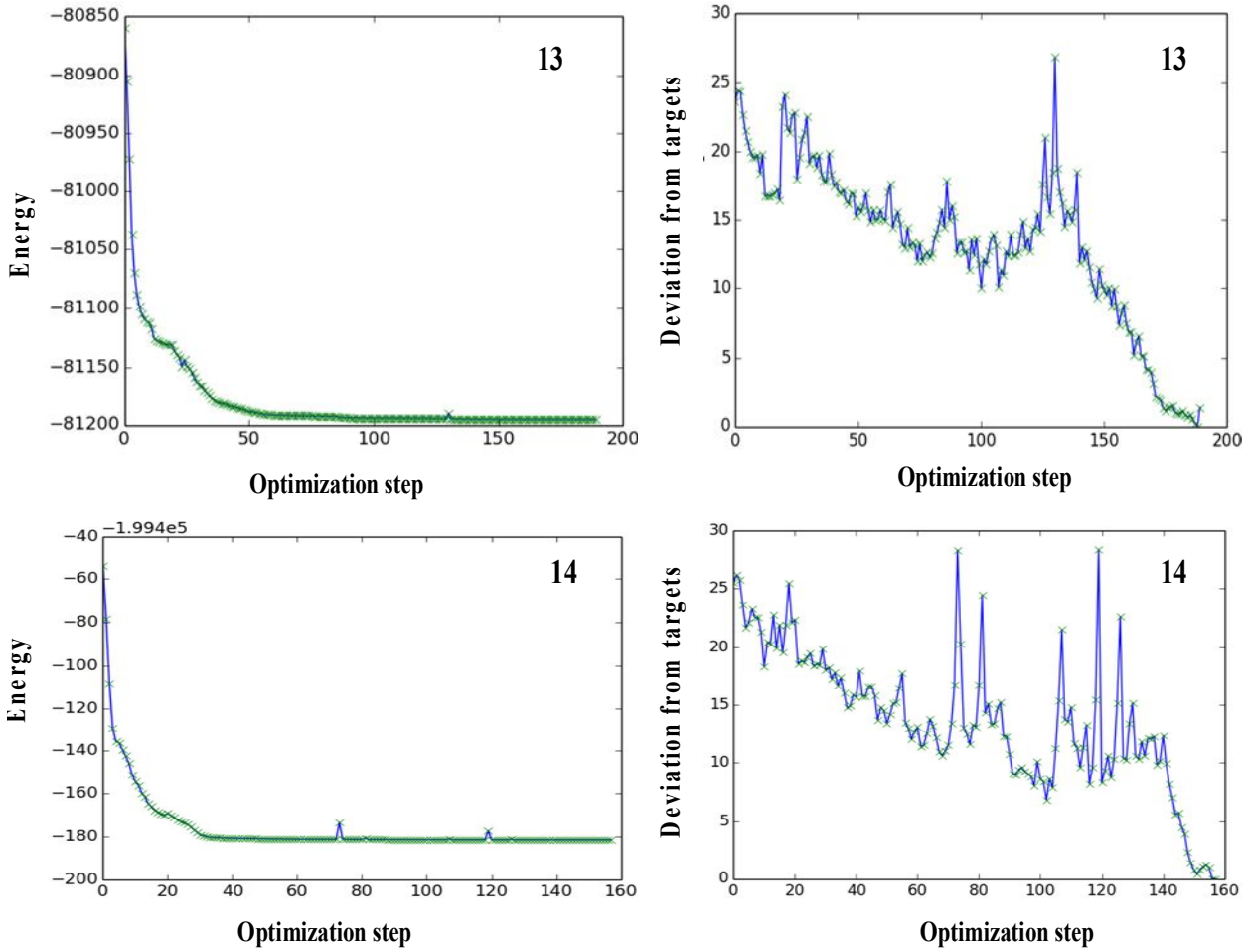

Fig. 3. Continued.

number of carbon atoms increased in the substituent. Similarly, derivatives (8-12) having various aliphatic chains (C2-C14) exhibited the progression of energy minimization with longer aliphatic substituent. Whereas, comparatively compounds (8-12) showed greater energy values compared to the derivatives (2-6) because of the additional myristoyl group of these derivatives. This analysis revealed that increment of molecular weight, *i.e*. bulky substituent, causes improvement of energy minimization. Compounds (7, 13 and 14) showed fluctuating values as these compounds were substituted by only aromatic groups (4-bromobenzoyl, methyl-tri-phenyl and 3-bromobenzoyl) but also affects molecular weight was observed. Compounds 13 exhibited the highest minimized energy among all the derivatives with highest molecular weight. The initial point (excited state) of energy minimization in all the plots was indicated by blue color and the final point (ground state) was visualized by green color. Moreover, lower deviation was observed for the designed derivatives compared to the parent drug parent ligand (1). The mode of deviation of derivatives (2-5) was observed almost in a same range, while derivatives (7-14) exhibited greater deviation. However, exceptionally derivative 6 showed maximum deviation during optimization and gave vastly zigzag plot. Finally, it can be proposed that substitution of different aliphatic and aromatic groups can affect the geometrical energy minimization and

Table 2. Molecular Weight (g mol^{-1}), Polarizability (a.u.), Heat Capacity (cal mol^{1}-kelvin), Entropy (cal mol^{-1}-kelvin) and Total Energy (Hartree).

Entry	Stoichiometry	Molecular weight	Polarizability	Heat capacity	Entropy	Electronic energy
1	$C_9H_{12}N_2O_6$	244.20	112.4993	61.530	133.206	-931.365
2	$C_{16}H_{15}O_7N_2Br$	427.20	196.7966	90.681	182.688	-1414.601
3	$C_{20}H_{19}O_9N_2Br$	511.80	240.9800	108.419	197.027	-4113.390
4	$C_{22}H_{23}O_9N_2Br$	555.37	264.1863	118.272	215.046	-4191.596
5	$C_{24}H_{27}O_9N_2Br$	567.34	283.7303	127.547	226.365	-4269.785
6	$C_{44}H_{67}O_9N_2Br$	847.91	491.9966	221.658	343.201	-5051.831
7	$C_{30}H_{21}O_9N_2Br_3$	793.21	363.1953	141.645	248.241	-9617.175
8	$C_{23}H_{38}O_7N_2$	454.56	214.3306	130.875	245.200	-1564.264
9	$C_{27}H_{42}O_9N_2$	538.63	298.2150	148.512	242.560	-1830.703
10	$C_{31}H_{50}O_9N_2$	594.74	346.1930	167.129	270.919	-1987.122
11	$C_{39}H_{66}O_9N_2$	706.95	425.7616	205.787	343.454	-2299.901
12	$C_{47}H_{82}O_9N_2$	819.16	513.7440	243.889	385.059	-2612.732
13	$C_{61}H_{66}O_7N_2$	939.19	600.4233	242.379	325.473	-2983.878
14	$C_{37}H_{44}O_9N_2Br_2$	820.56	427.1253	182.210	305.784	-7334.480

in this case molecular weight becomes a great factor. This result revealed that designed uridine esters are stable nearly to the parent compound uridine (1).

Thermodynamic Studies

A simple alteration of chemical structure significantly influences the structural properties including thermal and molecular orbital properties. Table 2 illustrates the stoichiometry, molecular weight, polarizability, heat capacity, electronic entropy and energy of uridine derivatives. Spontaneity of a reaction and stability of a product can be predicted from the free energy and enthalpy values [22]. Higher electronic energy values are more eligible for gaining thermal stability. In drug design, hydrogen bond formation and non-binding interactions are also influenced by dipole moment [22]. Comparatively, higher dipole moment can improve the binding property [23] of a ligand. Polarizability enhances probability the formation of covalent bonds. The most important factor affecting the polarizability of a substance is its size. Larger molecules are more polarizable than the smaller ones and we also found it in our study. Entropy plays an important role in determining the direction in which a chemical reaction spontaneously occurs. Heat capacity is helpful in determining the processing temperatures and the amount of heat necessary for processing and can be helpful in differentiating the polymeric composites. The values of all parameters increased gradually with increasing the length of the carbon chains of the substituent R1 when considering derivatives (2-6) and (8-12), and even more when this moiety contains an aromatic ring, and above all is for halogenated compounds as observed for the compounds (7, 13 and 14) (Fig. 2). It was observed that aromatic derivatives exhibit more improved electronic energy values

compared to the aliphatic ones. The highest electronic energy was observed for the derivative 7 (-9617.175 Hartree) among all derivatives. All derivatives presented higher absolute energy values than that of the parent ligand (1). Also, all aromatic uridine derivatives showed markedly improved polarizability. So, this discourse proved that modification of hydroxyl (-OH) groups of uridine significantly increases the thermodynamic parameters, indicating the inherent stability of the synthesized derivatives. Physicochemical data reported in Table 2 show that compound 13 with the higher molecular weight (939.19 g mol^{-1}) has the highest value of polarizability (600.4233 a.u.) among all derivatives. Whereas, the highest value of heat capacity (243.889 cal mol^{-1}-kelvin) and entropy (385.059 cal mol^{-1}-kelvin) were observed for compound (12). This analysis demonstrated that increase of molecular weight of uridine derivatives increases their stability [24]. Presence of bulky acylating groups also suggested the possible improvement of polarizability. However, it can be disclosed that all the synthesized uridine derivatives may show more stability than that of their parent structures.

Partial Atomic Charge

The partial atomic charge is essential for such purposes in molecular computations as a simplified representation of global charge distribution in a molecule and predicting its conformational behavior. To understand the charge distribution and the intrinsic property of the interactions in the designed structure, NBO analysis was carried out. Polarity of chemical bonds often influences the structure and reactivity of a molecule [25]. The molecular dipole moment is a vector which does not clearly define the polarity of the molecule. Different methods have been proposed for assigning partial charges to the interacting atoms within a molecule. The approaches of Mulliken Population Analysis and Natural Bond Orbital were employed to compute the partial charges of all drug interacting atoms [26]. They are the most popular analysis methods used. Dipole moment and molecular polarizability are related to atomic charges [27]. Here, all the hydrogen atoms showed positive charge in both methods and other electronegative atoms (N and O) showed negative charge in both methods as expected (Fig. 4). Compound 6 (C-1 and C-15) showed greater positive charge due to the presence of higher electronegative elements including oxygen (O-27, O-29 and O-31) and nitrogen (N-7), and H-5 exhibited the higher positive value than the other hydrogens because of the oxygen atom of hydroxyl group. Similarly, compound 13 (C-1, C-25 and C-40), compound 12 (C-1, C-21), and compound 14 (C-5, C-14) displayed positive charge in both methods due to the presence of oxygen atom of carbonyl group. Compound 13 (C-25) showed the highest positive charge among all other drugs due to the presence of greater electronegative nitrogen atom (N-10). As compounds (2-6) and (8-12) consist of aliphatic substituents and both derivatives 6 and 12 possess the longest carbon chain, these two derivatives showed the improved results. Again, compounds 7, 13 and 14 were modified by three aromatic rings (4-bromobenzoyl, methyl-tri-phenyl and 3-bromobenzoyl) and they exhibited almost similar results in charge distribution. Finally, we depicted compounds 6 and 13 (Fig. 4) from both aliphatic and aromatic series, as these compounds exhibited clear graphical view, while rest of the derivatives gave slightly scribble view.

Molecular Docking Studies

In order to predict the binding modes of uridine (1) and its modified derivatives, molecular docking were performed by Autodock Vina. Molecular docking is one of the most common methods used in structure based drug design to analyze the interaction between a small molecule and a protein at the atomic level. Afterward, all designated derivatives were docked into the same binding pocket of SARS-CoV-2 M^{pro} (PDB ID: 6Y84 and 6LU7) using similar optimized docking conditions to investigate their binding mode. The outcomes of docking carried out with the SARS-COV-2 main proteins 6Y84 and 6LU7 are shown in Tables 3 and 4, respectively. The analysis of the values showed that all derivatives of uridine displayed binding affinities ranging from -6.0 to -7.7 kcal mol^{-1} and from -6.2 to -7.8 kcal mol^{-1}, respectively, with the main proteases 6Y84 and 6LU7. All the binding affinities are negative indicating that the complex obtained is more stable than the ligand and receptor considered separately. The binding is all the stronger as the absolute value the bind affinity. Comparing the absolute values of binding affinities of the derivatives on the proteins shows that only the derivative 10

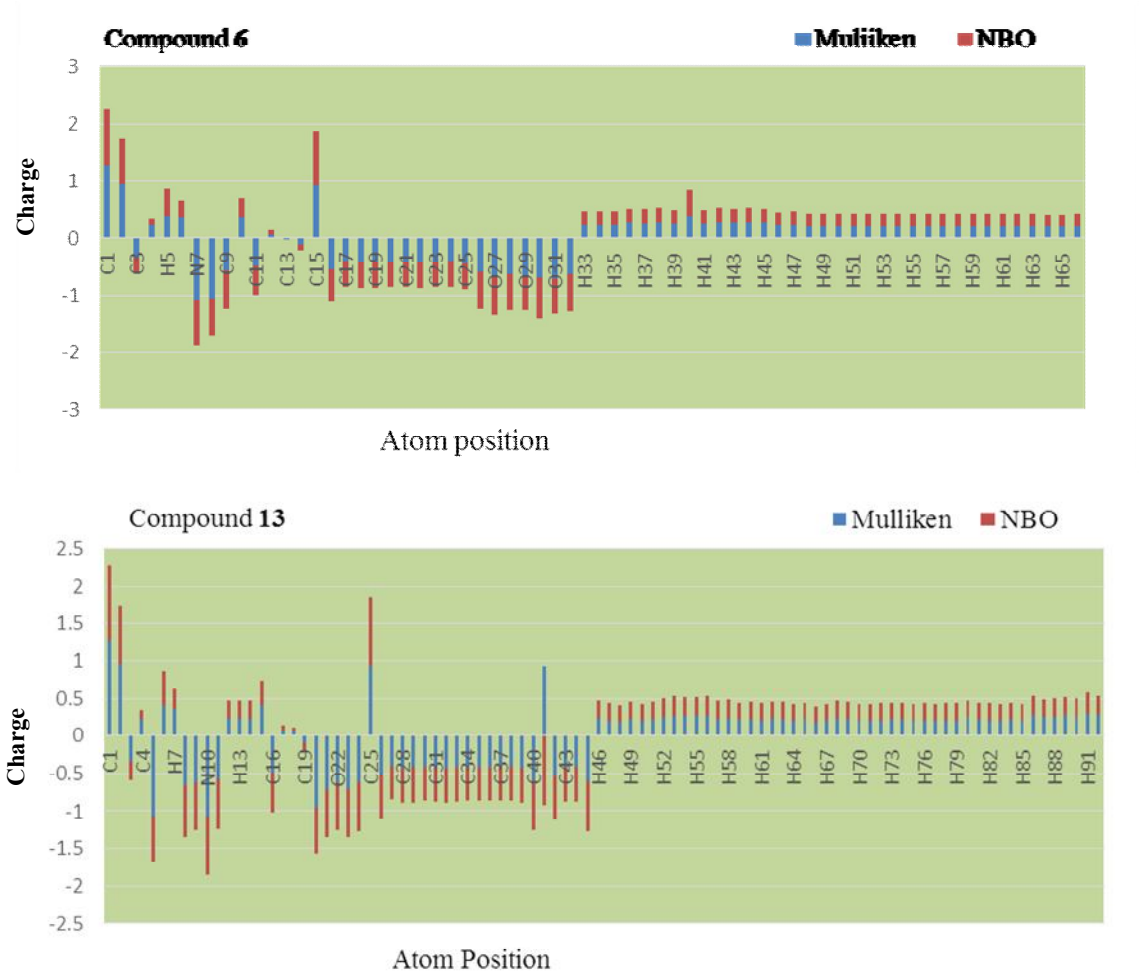

Fig. 4. Partial atomic charges of compounds 6 and 13.

has a lower value than that of the parent compound, uridine (1). In the case of protein 6Y84, the values of binding affinity are -5.9 kcal mol^{-1} for derivative 10 and -6.0 for uridine. In the case of protein 6LU7, the values are 6.0 kcal mol^{-1} for derivative 10 and -6.2 for uridine. These values were of the same order indicating that the substitutions carried out did not affect the binding affinity.

These results indicated that the modification of -OH group along with a long carbon chain and aromatic ring molecule increased the binding affinity, while addition of aromatic groups such as 4-bromobenzoyl, methyl-triphenyl and 3-bromobenzoyl made some fluctuations in binding affinities. However, modification with halogenated aromatic rings increased the binding affinity. The docked poses clearly exhibited that the drug molecules bind with the active sites of the SARS-CoV-2 M^{pro} macromolecular structure (Fig. 5). Figure 6 shows that aliphatic derivatives (2-6) bind firmly through conventional hydrogen bonds with residues CYS145, HIS41, HIS164, GLY143, SER144, LEU141, GLN110 and GLN189 besides other interactions such as carbon-hydrogen bonds (ASN142, GLN189 and HIS41), alkyl, pi-alkyl, pi-sigma and pi-pi stacked (MET49, CYS145, HIS41, THR25, MET165, TYR239 and PHE294) interactions. However, closer distance observed for GLY143 (1.81526 Å) and GLU166 (1.886456 Å) in the case of protease 6LU7, which indicated the tight binding of the ligand with the residues. Again, compounds (2 and 3) showed some electrostatic interactions such as pi-cation

Table 3. Binding Affinity (kcal mol^{-1}) and Nonbinding Interactions of Uridine and Its Derivatives with 6Y84

Entry	Protein	Binding affinity	Bond category	Residues in contact	Interaction types	Distance (Å)
1	6LU7	-6.2	Hydrogen	LEU141	H	2.466
			Hydrogen	SER144	H	2.535
			Hydrogen	SER144	H	2.711
			Hydrogen	GLU166	H	2.774
			Hydrophobic	HIS41	PPT	5.503
2	6LU7	-7.3	Hydrogen	SER46	H	2.264
			Hydrogen	SER46	H	2.755
			Hydrogen	GLY143	H	2.715
			Hydrogen	SER144	H	2.510
			Hydrogen	CYS145	H	2.275
			Hydrophobic	MET49	PS	3.847
3	6LU7	-6.9	Hydrogen	ALYS102	H	2.809
			Hydrogen	LYS102	H	2.473
			Hydrogen	GLN110	H	2.844
			Electrostatic	ASP153	PAn	3.886
			Hydrophobic	PHE294	PPS	3.806
			Hydrophobic	VAL104	PA	5.257
			Hydrophobic	PHE294	PA	4.197
4	6LU7	-6.3	Hydrogen	CYS145	H	2.431
			Hydrogen	GLY143	H	1.815
			Hydrogen	GLU166	H	2.036
			Hydrogen	GLU166	C	3.585
			Hydrophobic	PRO168	A	4.681
			Hydrophobic	ALA191	A	4.389
			Hydrophobic	PRO168	PA	5.142
5	6LU7	-7.3	Hydrogen	ASN142	H	2.969
			Hydrogen	GLY143	H	2.171
			Hydrogen	GLU166	H	1.864

Table 3. Continued

6	6Y84	-6.4	Hydrogen	ARG298	H	2.090
			Hydrogen	ARG298	H	3.017
			Hydrophobic	VAL104	PS	3.491
			Hydrophobic	PRO252	A	4.727
			Hydrophobic	PRO293	A	4.475
			Hydrophobic	PHE294	PA	3.971
7	6Y84	-7.7	Hydrogen	CYS145	H	2.854
			Hydrogen	THR190	H	2.415
			Hydrogen	GLN192	H	2.311
			Hydrogen	GLN189	C	3.657
			Hydrogen	HIS41	C	3.589
			Hydrophobic	MET49	PA	4.910
			Hydrophobic	MET165	PA	4.923
8	6Y84	-6.9	Hydrogen	GLU166	H	2.500
			Hydrogen	GLU166	H	2.017
			Hydrogen	GLN192	H	2.418
			Hydrogen	PRO168	C	3.682
			Hydrophobic	MET165	PA	4.842
			Hydrophobic	PRO168	PA	5.384
9	6Y84	-6.2	Hydrogen	ARG131	H	2.531
			Hydrogen	LEU287	H	2.206
			Electrostatic	ASP289	PAn	3.673
			Hydrophobic	LEU286	A	4.904
			Hydrophobic	TYR237	PA	5.051
10	6Y84	-5.9	Hydrogen	THR111	H	2.491
			Hydrogen	THR292	H	2.076
			Hydrophobic	VAL297	A	3.935
			Hydrophobic	PHE294	PA	4.561
11	6Y84	-6.1	Hydrogen	GLN110	H	2.830
			Hydrogen	THR111	H	2.804
			Hydrogen	THR111	H	2.789
			Hydrogen	THR292	H	2.335
			Hydrogen	ARG298	H	2.301
			Hydrophobic	PHE294	PS	3.988
			Hydrophobic	ILE249	A	5.222
			Hydrophobic	PRO293	A	3.961

Table 3. Continued

12	6Y84	-6.7	Hydrogen	THR111	C	2.587
			Hydrogen	SER158	C	2.264
			Hydrogen	THR292	C	2.180
			Hydrophobic	PHE294	PS	3.646
			Hydrophobic	ARG298	A	4.568
			Hydrophobic	VAL303	A	4.333
			Hydrophobic	ILE249	A	4.380
			Hydrophobic	PRO293	A	3.574
13	6Y84	-6.4	Hydrogen	THR199	H	2.015
			Hydrophobic	TYR237	PPT	5.165
			Hydrophobic	MET276	A	4.541
			Hydrophobic	LEU287	PA	4.944
			Hydrophobic	TYR239	PA	5.414
14	6Y84	-6.8	Hydrogen	ARG131	H	2.798
			Hydrogen	LEU287	H	2.412
			Hydrophobic	LEU286	PA	5.201
			Hydrophobic	TYR237	PA	4.951

N.B.: GLY = Glycine, TYR = Tyrosine, CYS = Cysteine, HIS = Histidine, ARG = Arginine, LEU = Leucine, MET = Methionine, THR = Threonine, PRO = Proline, ILE = Isoleucine, SER = Serine, PHE = Phenylalaine, VAL = Valine, GLN = Glutamine, ASN = Asparagine, LYS = Lysine, ALA = Alanine, GLU = Glutamic acid, ASP = Aspartic acid.

with ARG131 and pi-anion with ASP153, ASP289, and GLU290. This analysis indicated that aliphatic substituents can stabilizes the binding site and improve the binding affinity of uridine analogues with main protease. It is clear from the structural contrast compounds (2-6) have an additional aromatic (4-bromobenzoyl) substituent in the parent structure, high electron density in a compound leads to comparatively higher binding affinities (-7.2, -7.3, -6.8, -7.2 and -6.4 kcal mol^{-1} with 6Y84) and (-7.3, -6.9, -6.3, -7.3 and -6.4 kcal mol^{-1} with 6LU7). Again, derivatives (8-**12**) designed by various aliphatic chains (C2-C14) exhibited fluctuating binding affinities as the length of carbon chain increased. Compounds (10, 11 and 12) derivatives displayed an upward series of binding affinities (6Y84: -5.9 < -6.1 < -6.7 kcal mol^{-1} and 6LU7: -6.6 < -6.7 < -7.1 kcal mol^{-1}) with increasing their molecular weight except 8-9. Theses derivatives get stabilized by hydrogen bonding with GLN110, CYS145, ASP153, ARG131, THR111, ASN142, SER144, PHE140, hydrophobic bond MET165, TYR237, PHE294, ILE249, PRO293 and electrostatic bond ASP153, ASP289, GLU288 in both of 6LU7 and 6Y84. In the entire above docked pose, hydrogen bond plays a major role in the binding processes as could be observed from the respective 2D plots from (Fig. 6). Hydrogen displayed comparatively shorter bond distance in protein-ligand interaction, indicating the significant strength of hydrogen bond. It was found that for aliphatic compounds (2-6) and (8-12) molecular weight can affect the binding affinity and protein ligand interaction as it is increased with the length of the substituents. Finally, aromatic substituted compounds (7, 13, and 14**)** displayed the highest binding affinities (-7.7, -6.8 and -7.8 kcal mol^{-1}) and similar binding site for both of the protease proteins 6Y84 and 6LU7. Theses inhibitors binding site with the

Table 4. Binding Affinity (kcal mol^{-1}) and Nonbinding Interactions of Uridine and Its Derivatives with 6LU7

Entry	Protein	Binding affinity	Bond category	Residues in contact	Interaction types	Distance (Å)
1	6LU7	-6.2	Hydrogen	LEU141	H	2.466
			Hydrogen	SER144	H	2.535
			Hydrogen	SER144	H	2.711
			Hydrogen	GLU166	H	2.774
			Hydrophobic	HIS41	PPT	5.503
2	6LU7	-7.3	Hydrogen	SER46	H	2.264
			Hydrogen	SER46	H	2.755
			Hydrogen	GLY143	H	2.715
			Hydrogen	SER144	H	2.510
			Hydrogen	CYS145	H	2.275
			Hydrophobic	MET49	PS	3.847
3	6LU7	-6.9	Hydrogen	ALYS102	H	2.809
			Hydrogen	LYS102	H	2.473
			Hydrogen	GLN110	H	2.844
			Electrostatic	ASP153	PAn	3.886
			Hydrophobic	PHE294	PPS	3.806
			Hydrophobic	VAL104	PA	5.257
			Hydrophobic	PHE294	PA	4.197
4	6LU7	-6.3	Hydrogen	CYS145	H	2.431
			Hydrogen	GLY143	H	1.815
			Hydrogen	GLU166	H	2.036
			Hydrogen	GLU166	C	3.585
			Hydrophobic	PRO168	A	4.681
			Hydrophobic	ALA191	A	4.389
			Hydrophobic	PRO168	PA	5.142
5	6LU7	-7.3	Hydrogen	ASN142	H	2.969
			Hydrogen	GLY143	H	2.171
			Hydrogen	GLU166	H	1.864
6	6LU7	-6.4	Hydrogen	LYS102	H	2.087
			Hydrogen	GLN110	H	2.098
			Hydrogen	GLN110	H	3.020
			Hydrogen	ASN151	H	2.475
			Hydrogen	SER158	C	3.603
			Hydrophobic	ILE249	A	5.113
			Hydrophobic	VAL104	PA	3.985
			Hydrophobic	VAL104	PA	5.101
			Hydrophobic	PHE8	PA	5.304
			Hydrophobic	PHE294	PA	4.502

Table 4. Continued

7	6LU7	-7.8	Hydrogen	LEU141	H	2.118
			Hydrogen	GLY143	H	2.307
			Hydrogen	GLY143	H	2.266
			Hydrogen	SER144	H	2.451
			Hydrogen	SER144	H	2.955
			Hydrogen	CYS145	H	2.364
			Hydrogen	CYS145	H	2.838
			Hydrogen	GLN189	C	3.444
			Hydrophobic	CYS145	A	5.273
			Hydrophobic	MET165	PA	4.548
			Hydrophobic	CYS145	PA	4.674
8	6LU7	-6.3	Hydrogen	ASP289	H	2.737
			Hydrogen	LYS5	H	2.760
			Hydrogen	LYS137	H	2.916
			Hydrogen	LYS137	H	2.539
			Hydrogen	THR199	H	2.235
			Hydrogen	ASP289	C	3.264
			Hydrogen	ASP289	C	3.752
			Electrostatic	GLU288	PAn	3.868
9	6LU7	-6.5	Hydrogen	PHE140	H	2.262
			Hydrogen	ASN142	H	2.808
			Hydrogen	SER144	H	2.276
			Hydrogen	SER144	H	2.538
			Hydrogen	CYS145	H	2.308
			Hydrogen	GLU166	H	2.923
			Hydrogen	GLN189	C	3.320
10	6LU7	-6.0	Hydrogen	ASP248	H	2.960
			Hydrogen	GLN110	H	2.988
			Hydrogen	GLN110	H	1.904
			Hydrogen	PHE294	H	2.611
			Hydrophobic	ILE249	A	4.904
			Hydrophobic	PRO293	A	5.490
			Hydrophobic	ILE249	PA	3.991
			Hydrophobic	PHE294	PA	4.237
11	6LU7	-6.6	Hydrogen	GLN110	H	2.153
			Hydrogen	ASN151	H	2.929
			Hydrogen	SER158	H	2.150
			Electrostatic	ASP153	H	3.838
			Hydrophobic	VAL202	PAn	4.876
			Hydrophobic	ILE249	A	4.822
			Hydrophobic	PRO293	A	3.897
			Hydrophobic	PRO293	A	4.804

Table 4. Continued

			Hydrophobic	VAL297	A	4.478
			Hydrophobic	HIS246	A	4.753
			Hydrophobic	PHE294	PA	4.336
12	6LU7	-6.7	Hydrogen	THR111	H	2.335
			Hydrogen	THR292	H	2.147
			Hydrogen	ASP153	C	3.442
			Hydrophobic	VAL202	A	4.759
			Hydrophobic	PHE294	PA	5.031
13	6LU7	-7.1	Hydrophobic	ILE249	PS	3.547
			Hydrophobic	ILE249	PS	3.867
			Hydrophobic	PHE294	PPS	4.397
			Hydrophobic	ILE106	A	4.842
			Hydrophobic	PHE294	PA	3.931
			Hydrophobic	PRO293	PA	4.353
14	6LU7	-7.0	Hydrogen	HIS163	H	2.889
			Hydrogen	ASN142	H	2.286
			Hydrogen	GLY143	H	2.743
			Hydrogen	SER144	H	2.307
			Hydrogen	SER144	H	2.427
			Hydrogen	CYS145	H	2.322
			Hydrogen	GLU166	H	2.130
			Hydrogen	ASN142	C	3.057
			Hydrophobic	MET165	A	5.131
			Hydrophobic	PRO168	PA	3.946
			Hydrophobic	CYS145	PA	4.732
			Hydrophobic	HIS41	PA	5.198

H = Conventional Hydrogen Bond; C = Carbon Hydrogen Bond; A = Alkyl; PA = Pi-Alkyl; PAn = Pi-Anion; PCa = Pi-Cation; PS = Pi-Sigma; PPS = Pi-Pi Stacked; PPT = Pi-Pi T-Shaped.

protease of SARS-CoV-2 consists of residues HIS41, MET49, GLY143, CYS145, HIS163, HIS164, SER144, ASN142, GLU166, PRO168 and GLN189 and it was evident from the recent study on the a-ketoamide inhibitors for SARS-CoV-2 main protease [28].

Compound 13 displayed a new type of hydrophobic interaction; *i.e.*, pi-pi T-shaped for TYR237. Among these three derivatives, compound 13 possess six additional benzene rings, however, it showed lower binding energy compared to the other two compounds. So, it may suggest that halogenated aromatic ring (4-bromobenzoyl and 3-bromobenzoyl) impacts the drug properties and is responsible for governing uridine derivative's inhibitor potency which in turn is a direct measure of the potency of the drug. It was observed that most of the interactions were hydrophobic in nature in the case of longer carbon chain. So, it may consider as comparatively less polar than others. It was found that utmost derivatives displayed hydrophobic interactions with PHE294. Besides, compounds (3, 6 and 13) displayed the maximum π-π interactions with PHE294 denoting the tight binding active site. The above results suggested that PHE294 is considered as the main component of the PPS and PPT, responsible for the accessibility of small molecules to the active site. Binding

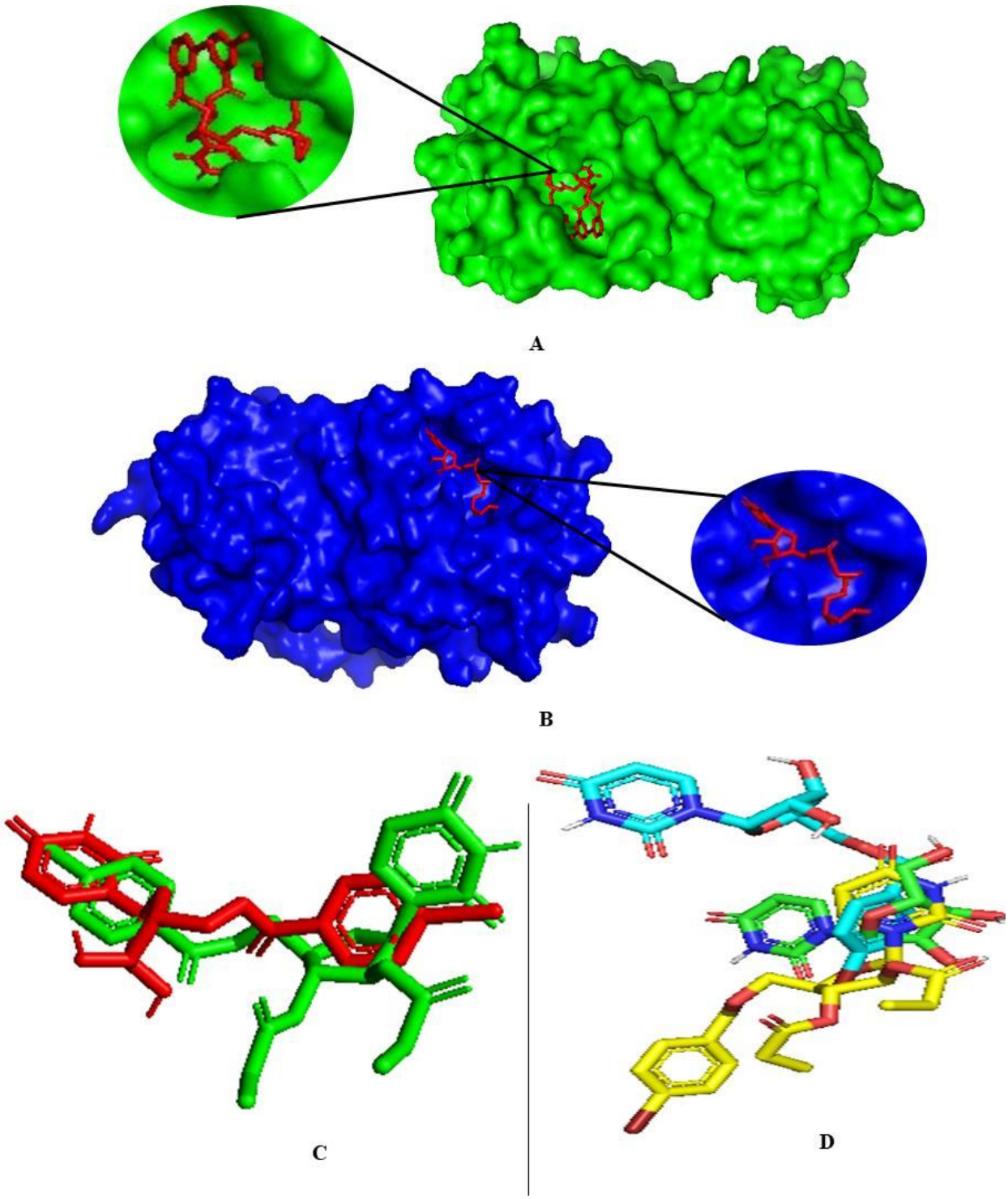

Fig. 5. Docked conformation of compound (7) at inhibition bonding site of 6LU7 (A), 6Y84 (B), and superimposed views of compounds after rigid docking with 6Y84 (C), and 6LU7 (D), which exhibited the highest binding affinities, -7.7 kcal mol^{-1} and -7.8 kcal mol^{-1}.

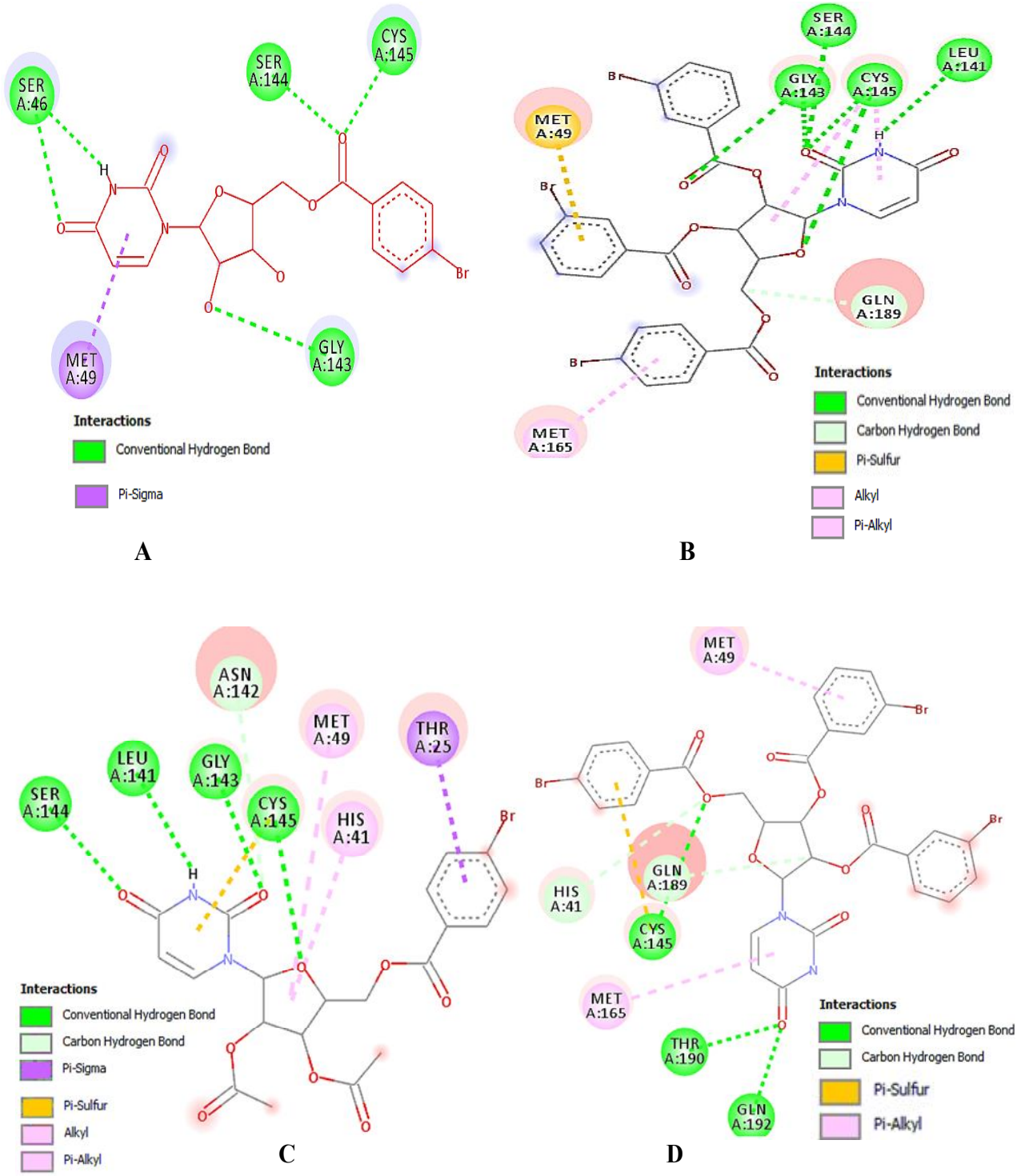

Fig. 6. Non-binding interactions of compounds 2 (A) and 7 (B) with the amino acid residues of 6LU7, compounds 3 (C), and 7 (D) with the amino acid residues of 6Y84 made by Discovery Studio.

affinity and binding specialty were increased in the case of (6Y84: 2-9 and 11-13, and 6LU7: 2-6, 8-12, and 7, 13, 14) due to effective hydrogen bonds. It was found that the modification of -OH group of uridine (1) increases the π-π interactions with the residues of the active site, while increasing their polarity results in the formation of hydrogen bonding interactions. The maximum numbers of H-bonds were obtained for the compounds (7, 8, 9 and 14) in case of protease 6LU7 forming with CYS145, GLY143, HIS163, ASN142, SER144, GLN189 and GLU166 residues. In contrast, compounds (2, 4, 6 and 10) formed similar numbers of H-bonds with different residues during interaction with 6LU7. Moreover, these compounds showed similar H-bond interactions with CYS145, GLY143, SER144, GLN110 despite having different bonding distances. On the contrary, during 6Y84 interactions, compounds (2, 3, 7, 8 and 11) displayed the maximum numbers of hydrogen bond with the same residues as found for 6LU7 except a few differences such as THR111, THR199, HIS41, GLU288 and GLN192. Hydrogen-bonds showed a vital function in shaping the specificity of ligand binding with the receptor, drug design in chemical and biological processes, molecular recognition and biological activity [29].

Hydrogen bond surface compounds (7 and 9) and hydrophobic surface compounds (5 and 11) with both protease proteins are respectively represented in Figs. 7 and 8. Although compounds (5 and 11) showed few numbers of hydrogen type non-bonding interaction, they have a significant range of hydrophobicity due to having hetero aromatic ring [30]. We observed from the blind docking study of all the thirteen uridine derivatives with the SARS-CoV-2 protease that the molecules are generally surrounded by the above mentioned residues, clearly suggesting that this molecule can prevent the viral replication of SARS-CoV-2. The distance of the ligands along with the change in accessible area of the two important catalytic residues (HIS41 and CYS145) within the active site of the protease is shown in Tables 3 and 4. The calculated binding affinities varied in the range of (-5.9 to -7.7 kcal mol^{-1} with 6Y84) and (-6.0 to -7.8 kcal mol^{-1} with 6LU7), suggesting that the molecules can spontaneously interact with the binding site of SARS-CoV-2 M^{pro}.

Although the blind docking studies reveals that all the molecules can act as potential agents for COVID treatments, from the estimated free energy of binding values (Tables 3 and 4), we can infer that derivative 7 with the highest negative minimum binding energy value -7.7 and -7.8 kcal mol^{-1} among all the studied compounds can be the best possible SARS-CoV-2 inhibitor. So, it was resolved that most of the selected uridine derivatives show promising activities and could be use to design effective antiviral drugs against SARSCoV-2.

In Silico Pharmacokinetic Analysis

It was evident that all the modified uridine derivatives have the significant potential activities. Therefore, in order to ensure that the modified compounds are the viable drugs, we used the *in silico* pharmacokinetic parameters ADMET and drug-likeness.

The pkCSM online server [31] was employed to calculate *in silico* ADMET properties (Table 5). The absorbance value below 30% indicated poor absorbance. Most of the designed molecules displayed a value above 80%, indicating a good absorbance in the human intestine. Volume of distribution (VDss) is thought to be high if the value is higher than 0.45. In addition, blood-brain barrier (BBB) and central nervous system (CNS) permeability standard values (> 0.3 to < -1 logBB and > -2 to < -3logPS), respectively. For a given compound, a logBB < -1 is poor distributed to brain, while logBB > 0.3 is potential to cross BBB and logPS > -2 considered to penetrate the CNS, while logPS < -3 is difficult to move in the CNS [32]. It was observed that most of the compounds have the significant potential to cross the barriers except compounds (2, 9 and 7). The enzymatic metabolism ensures the chemical biotransformation of a designed drug in the body, which plays a key role in transformation of drug compounds. In the body, drugs produce several enzymatic metabolites contributing in catalyzing the reaction with various drug concentrations [33]. It is important to consider their metabolism, which may show various physicochemical and pharmacological parameters. The cytochrome P450 (CYP450) plays a major role in drug metabolism because the major liver enzyme system is involved in phase 1 metabolism. Some selective CYP genes, including CYP1, CYP2, CYP3 and CYP4, were found to be involved in drug metabolism with CYP (1A2, 2C19, 2D6 and 3A4) which

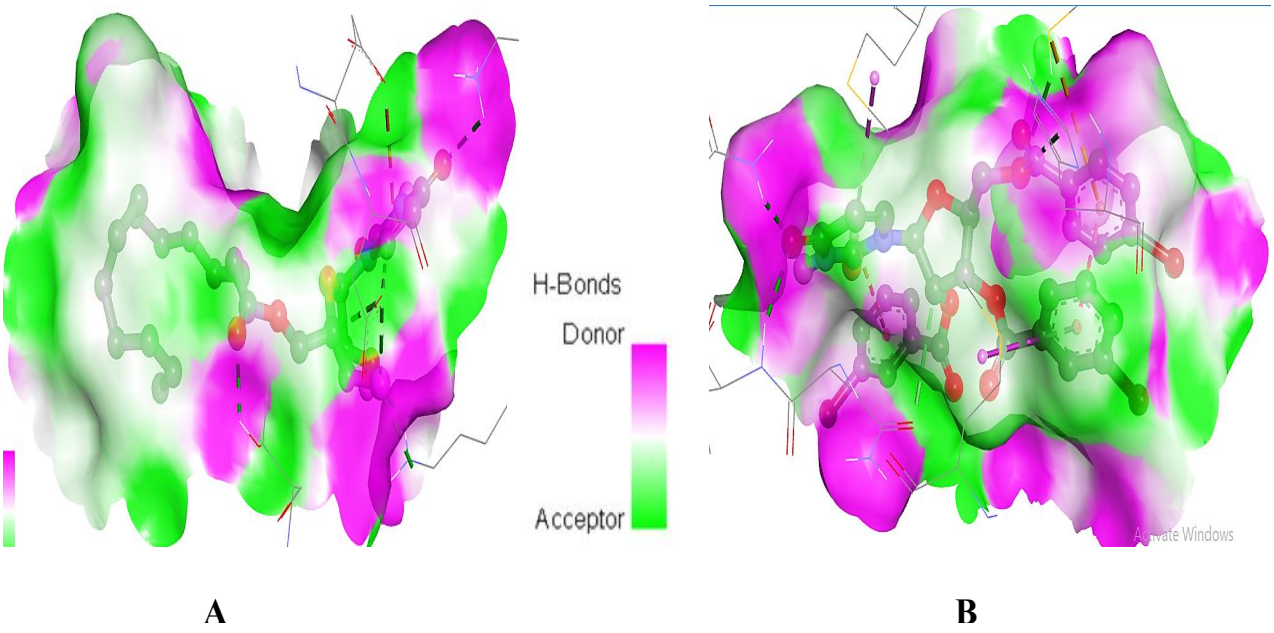

Fig. 7. Hydrogen bond surface of 6LU7 with compound 9 (A) and 6Y84 with compound 7 (B).

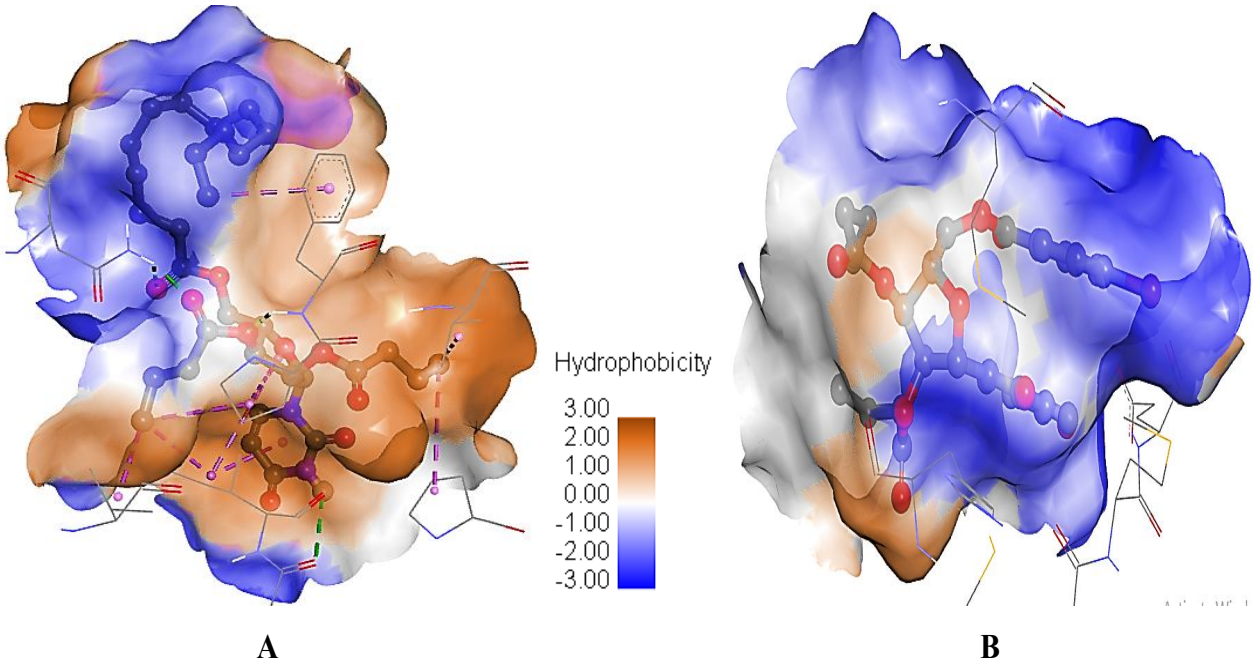

Fig. 8. Hydrophobic bond surface of 6LU7 with compound 11 (A) and 6Y84 with compound 5 (B).

Table 5. *In Silico* ADMET Prediction of Uridine and Its Derivatives

Entry	Absorption		Distribution		Metabolism						Excretion	Toxicity
	Intestinal absorption (human)	VDss (human)	BBB permeability	CNS permeability	Substrate		Inhibitor				Total Clearance	AMES toxicity
					CYP							
					2D6	3A4	1A2	2C19	2D6	3A4		
	Numeric (%Absorbed)	Numeric (logL/kg)	Numeric (logBB)	Numeric (logPS)	Categorical (Yes/No)						Numeric (log ml/min/kg)	Categorical (Yes/No)
1	45.878	0.304	-0.899	-4.570	No	Yes	No	No	No	Yes	0.771	No
2	59.929	0.448	-0.154	-3.419	No	Yes	No	Yes	No	Yes	-0.144	No
3	76.469	0.459	0.086	-2.441	No	Yes	Yes	Yes	No	Yes	-0.218	No
4	81.241	0.463	0.183	-2.394	No	Yes	Yes	Yes	No	Yes	-0.150	No
5	83.009	0.476	0.156	-1.215	No	Yes	Yes	Yes	No	Yes	-0.212	No
6	97.938	0.544	0.258	-0.584	No	Yes	Yes	Yes	No	Yes	0.423	No
7	83.595	0.484	0.389	-1.140	No	Yes	Yes	Yes	No	Yes	-0.467	No
8	59.128	0.346	-0.403	-4.533	No	Yes	No	Yes	No	Yes	1.768	No
9	62.905	0.413	-0.077	-4.519	No	Yes	No	Yes	No	Yes	1.287	No
10	70.766	0.432	0.052	-3.067	No	Yes	Yes	Yes	No	Yes	1.392	No
11	77.777	0.446	0.108	-2.388	No	Yes	Yes	Yes	No	Yes	1.539	No
12	83.681	0.487	0.198	-2.148	No	Yes	Yes	Yes	No	Yes	1.676	No
13	99.71	0.568	0.477	-0.765	No	Yes	Yes	Yes	No	Yes	0.075	No
14	84.566	0.533	0.179	-1.219	No	Yes	Yes	Yes	No	Yes	0.025	No

causes the biotransformation of greater than 90% of drugs undergoing phase I metabolism. Therefore, among these members, CYP3A4 is the most important inhibitor [34]. All newly designed compounds were found to be the substrate and the inhibitor of CYP3A4. Clearance is a constant that indicates the relationship between drug concentration in body and the rate of elimination of drug. Therefore, all modified derivatives showed a somewhat high value, but still acceptable in persistence of the drug in body.

Furthermore, it is necessary to examine whether the calculated compounds are non-toxic, because this plays a critical role in the selection of drugs. All the compounds designed in this study are non-toxic. Overall, compounds (3-7) and (10-14) have better *in silico* pharmacokinetic properties. The modified uridine derivatives were evaluated with the SwissADME web tool for their drug-likeness and pharmacokinetics properties which are crucial for rational drug design. Generally, drug-likeness is evaluated using

Table 6. Drug-Likeness Parameters of Uuridine and Its Derivatives

Entry	Molar refractivity (Å)	log$P_{o/w}$ (XLOGP3)	NRB	NHA	NHD	TPSA (Å²)	Csp3
1	55.85	-2.13	2	6	4	130.83	0.56
2	90.61	0.39	5	7	3	130.85	0.31
3	111.08	1.87	9	9	1	142.99	0.35
4	127.62	3.64	10	9	1	142.99	0.43
5	130.31	2.87	13	9	1	142.99	0.46
6	226.45	13.70	33	9	1	142.99	0.70
7	166.29	5.92	11	9	1	142.99	0.17
8	121.69	4.29	16	7	3	130.85	0.78
9	141.16	5.77	20	9	1	142.99	0.74
10	160.39	7.42	24	9	1	142.99	0.77
11	198.85	11.76	32	9	1	142.99	0.82
12	237.30	16.09	40	9	1	142.99	0.85
13	277.84	14.38	26	7	1	108.85	0.33
14	196.37	9.81	22	9	1	142.99	0.49

Here, NHD = No. of H-bond donors; NHA = No. of H-bond acceptor; NRB = No. of rotatable bonds; TPSA = Topological polar surface area; Csp3 = fraction of sp3 carbon atom.

Lipinski's rule of five [35]. As a matter of priciple, an orally active drug should have no more than one interruption of the following conditions: (1) no more than five hydrogen bond donors, (2) no more than ten hydrogen bond acceptors, (3) molecular mass of less than 500 Da and (4) an octanol-water partition coeffecient of not more than five. If two or more of the guidelines are disrupted, reduced absorption can be estimated. All of nucleoside ligands do not violate any of the Lipinski's rule of five (Table 6).

However, topological polar surface area (TPSA) is likewise employed as a contributing factor for oral absorption and blood-brain barier permeation capacity and the screened drug-likeness of a molecule should have TPSA between 20 and 130 Å². The SwissADME web tool predication raveled that some of the ligands violate only this standard except 1, 2, 8 and 13 which are anticipated to be orally bioavailable.

CONCLUSIONS

In summary, quantum calculations, atomic partial charge, molecular docking, and SwissADME tools were successfully employed to determine the best uridine derivatives as the potential drugs against the main protease of SARS-CoV-2. Among the fourteen compounds studied, derivatives 2, 3, 4, 5, 7, 9 and 14 showed the highest binding affinities and strong interactions with both or at least one of the catalytic residues (CYS145 and HIS41) of the main protease. These compounds showed many non-covalent interactions, such as hydrogen bonding,

hydrophobic and electrostatic interactions and displayed more interesting drug-like properties than the parent ligand, uridine. These blind molecular docking studies suggested a potential approach for the application of anti-fungal, and anti-bacterial drugs as expected inhibitors of SARS-CoV-2 M^{pro}, a pandemic and a global threat that is currently affecting millions of people, leading to death in excessive cases. The combination of ADMET prediction and drug-likeness has shown promising results *in silico*, because the newly designed molecules have improved kinetic properties and most of them comply with all conditions of drug-likeness rules as well as a magnificent result in terms of biological activity. Finally, this research may be useful to understand the chemical, thermal, physicochemical, biological, and pharmacokinetic properties of modified uridine derivatives.

ACKNOWLEDGMENTS

The authors are grateful to the *Research & Publication Office, University of Chittagong*, Bangladesh for providing financial support to carry out this piece of research.

Declaration of Interest

The authors declare no conflict of interest.

Author Contributions

S.M.A.K and M.A.H coordinated the study. J.M., M.A.H, A.A., K.M.R. carried out design and molecular docking studies and S.M.A.K., Y.F. and Y.O. contributed to the writing and editing of the manuscript.

REFERENCES

[1] Xiao-huan, L.; Xiao, Z.; Zhen-hua, L.; You-shuang, Z.; Tao, W., Potential molecular targets of nonstructural proteins for the development of antiviral drugs against SARS-CoV-2 infection. *Biomed. Pharmacother.* **2021**, *133*, 1-19, DOI: 10.1016/j.biopha.2020.111035.

[2] Bulbul, M. Z. H.; Hosen, M. A.; Ferdous, J.; Chowdhury, T. S.; Misbah, M. M. H.; Kawsar, S. M. A., DFT study, physicochemical, molecular docking and ADMET predictions of some modified uridine derivatives. *Int. J. New Chem.* **2021**, *8*, 88-110, DOI: 10.22034/ijnc.2020.131337.1124.

[3] De Clercq, E.; Li, G., Approved antiviral drugs over the past 50 years. *Clin. Microbiol. Revi.* **2016**, *29*, 695-747, DOI: 10. 1128/CMR.00102-15.

[4] Geiger, A.; Yamasaki, S.; Cytidine and uridine requirement of the brain. *J. Neurochem.* **1956**, *1*, 93-100, DOI: 10.1111/j.1471-4159.1956.tb12059.x.

[5] Gasser, T.; Moyer, J. D.; Handschumacher, R. E., Novel single-pass exchange of circulating uridine in rat liver. *Science*, **1981**, *213*, 777-778, DOI: 10.1126/science.7256279.

[6] Chen, S.; Fukuda, M., Cell type-specific roles of carbohydrates in tumor metastasis. *Methods Enzymol.* **2006**, *416*, 371-380, DOI: 10.1016/S0076-6879(06)16024-3.

[7] Oh , J. Y.; In, Y. S.; Kim, M. K.; Ko, J. H.; Lee, H.; Shin, K. C.; Lee, S. M.; Wee, W. R.; Lee, J. H.; Park, M.; Protective effect of uridine on cornea in a rabbit dry eye model. *Invest. Ophthalmol. Vis. Sci.* **2007**, *48*, 1102-1109, DOI: 10.1167/iovs.06-0809.

[8] Kawsar, S. M. A.; Hosen, M. A.; Fujii, Y.; Ozeki, Y., Thermochemical, DFT, molecular docking and pharmacokinetic studies of methyl β-D-galactopyranoside esters. *J. Comput. Chem. Mol. Model.* **2020**, *4*, 452-462, DOI: 10.25177/JCCMM.4.4.RA.10663.

[9] Seeberger, P. H.; Werz, D. B., Synthesis and medical applications of oligosaccharides. *Nature*, **2007**, *446*, 1046-1051, DOI: 10.1038/nature05819.

[10] Lu, H., Drug treatment options for the 2019-new coronavirus (2019-nCoV). *Biosci. Trends,* **2020**, *14*, 69-71, DOI: 10.5582/bst.2020.01020.

[11] Gaussian, R. A.; Frisch, M. J.; Trucks, G. W.; Schlegel, H. B.; Scuseria, G. E. *et al*. Gaussian Inc., Wallingford CT, **2009**, https://gaussian.com/g09citation/.

[12] Becke, A. D., Density-functional exchange-energy approximation with correct asymptotic behaviour. *Phys. Rev. A,* **1988**, *38*, 3098-3100, DOI: 10.1103/PhysRevA.38.3098.

[13] Lee, C.; Yang, W.; Parr, R. G., Development of the colle-Salvetti correlation-energy formula into a functional of the electron density. *Phys. Rev. B,* **1988**,

37, 785-789, DOI: 10.1103/PhysRevB.37.785.

[14] Pearson, R. G., Absolute electronegativity and hardness correlated with molecular orbital theory. *Proc. Natl. Acad. Sci.* **1986**, *83*, 8440-8441, DOI: 10.1073/pnas.83.22.8440.

[15] Ferreira, L. L. G.; Andricopulo, A. D., ADMET modeling approaches in drug discovery. *Drug Discov. Today*, **2019**, *24*, 1157-1165, DOI: 10.1016/ j.drudis.2019.03.015.

[16] Daina, A.; Michielin, O.; Zoete, V., SwissADME: A free web tool to evaluate pharmacokinetics, drug-likeness and medicinal chemistry friendliness of small molecules. *Sci. Rep*. **2017**, *7*, 1-13, DOI: 10.1038/ srep42717.

[17] Berman, H. M.; Westbrook, J.; Feng, Z.; Gilliland, G.; Bhat, T. N.; Weissig, H., The protein data bank. *Nucleic Acids Res.* **2000**, *28*, 235-242, DOI: 10.1093/ nar/28.1.235.

[18] Delano, W. L., The PyMOL molecular graphics system. De-Lano Scientific, San Carlos, CA, USA, **2002**.

[19] Guex, N.; Peitsch, M. C., Swiss-model and the Swiss-Pdb viewer: An environment for comparative protein modeling. *Electrophoresis*, **1997**, *18*, 2714-2723, DOI: 10.1002/elps.1150181505.

[20] Dallakyan, S.; Olson, A. J., Small-molecule Library Screening by Docking with Py Rx. In: Hempel, J. E.; Williams, C. H.; Hong, C. C. (Eds.), Chemical Biology: Methods and Protocols. Springer New York, USA, **2015**, pp. 243-250.

[21] Version ADS 4.0, Accelrys, San Diego, USA, **2017**.

[22] Cohen, N.; Benson, S. W., Estimation of heats of formation of organic compounds by additivity methods. *Chem. Rev.* **1993**, *93*, 2419-2438, DOI: 10.1021/cr00023a005.

[23] Lien, E. J.; Guo, Z. R.; Li, R. L.; Su, C. T., Use of dipole moment as a parameter in drug-receptor interaction and quantitative structure-activity relationship studies. *J. Pharm. Sci.* **1982**, *71*, 641-655, DOI: 10.1002/jps.2600710611.

[24] Kawsar, S. M. A.; Hosen, M. A., An optimization and pharmacokinetic studies of some thymidine derivatives. *Turk. Comput. Theor. Chem.* **2020**, *4*, 59-66, DOI: 10.33435/tcandtc.718807.

[25] Heinz, H.; Suter, U. W., Atomic charges for classical simulations of polar systems. *J. Phys. Chem. B,* **2004**, *108*, 18341–18352, DOI: 10.1021/jp048142t.

[26] Gross, K. C.; Seybold, P. G.; Hadad, C. M., Comparison of different atomic charge schemes for predicting pKa variations in substituted anilines and phenols. *Int. J. Quantum Chem.* **2002**, *90*, 445-58, DOI: 10.1002/qua.10108.

[27] Mulliken, R. S., Electronic population analysis on LCAO-MO molecular wave functions. *I. J. Chem. Phys.* **1955**, *23*, 1833-1840, DOI: 10.1063/1.1740588.

[28] Zhang, L., Lin, D., Sun, X., Curth, U., Drosten, C., Sauerhering, L., Hilgenfeld, R., Crystal structure of SARS-CoV-2 main protease provides a basis for design of improved a-ketoamide inhibitors. *Science*, **2020**, *368*, 409-412, DOI: 10.1126/science.abb3405.

[29] Perlstein, J., The weak hydrogen bond in structural chemistry and biology. *J. American Chem. Soc.* **2001**, *123*, 191-192, DOI: 10.1021/ja0047368.

[30] Jannatul, M.; Asraful, A.; Kazi, M. R.; Sujan, D.; Anowar, H.; Yuki, F.; Imtiaj, H.; Yasuhiro, O.; Kawsar, S. M. A., Synthesis, characterization, synergistic antimicrobial properties and molecular docking of sugar modified uridine derivatives. *Ovidius Univ. Annals Chem.* **2021**, *32*, 6-21, DOI: 10.2478/auoc-2021-0002.

[31] Pires, D. E. V.; Blundell, T. L.; Ascher, D. B., pkCSM: predicting small-molecule pharmacokinetic and toxicity properties using graph-based signatures. *J. Med. Chem.* **2015**, *58*, 4066-4072, DOI: 10.1021/ acs.jmedchem.5b00104.

[32] Clark, D. E., In silico prediction of blood-brain barrier permeation. *Drug Discov. Today*, **2003**, *8*, 927-933, DOI: 10.1016/s1359-6446(03)02827-7.

[33] Kok-Yong, S.; Lawrence, L., Drug Distribution and Drug Elimination. Basic Pharmacokinetic Concepts some Clinical Applications, InTechOpen, London, SW7 2QJ, UK, **2015**, DOI: 10.5772/59929.

[34] Thapar, M. M., Pharmacokinetics and Dynamics of Atovaquone and Proguanil, Malarone®, Karolinska University Press, Stockholm, Sweden, **2004**, http://hdl.handle.net/10616/43294.

[35] Lipinski, C. A.; Lombardo, F.; Dominy, B. W.; Feeney, P. J., Experimental and computational approaches to estimate solubility and permeability in drug discovery and development. *Adv. Drug Deliv. Rev.* **2001**, *46*, 3-26, DOI: 10.1016/s0169-409x(00)00129-0.